Princeton Plasma Physics Laboratory

PPPL-

PPPL-

PRINCETON PLASMA PHYSICS LABORATORY

Princeton Plasma Physics Laboratory
Report Disclaimers

PPPL Report Availability

Princeton Plasma Physics Laboratory:

http://www.pppl.gov/techreports.cfm

Office of Scientific and Technical Information (OSTI):

http://www.osti.gov/bridge

Related Links:

U.S. Department of Energy

Office of Scientific and Technical Information

Fusion Links

Finite-β Simulation of Microinstabilities

Edward A. Startsev and W. W. Lee

Princeton Plasma Physics Laboratory, Princeton University, Princeton, NJ 08543

Abstract

A new split-weight perturbative particle simulation scheme for finite-β plasmas in the presence of background inhomogeneities is presented. The scheme is an improvement over the original split-weight scheme, which splits the perturbed particle response into adiabatic and non-adiabatic parts to improve numerical properties. In the new scheme, by further separating out the adiabatic response of the particles associated with the quasi-static bending of the magnetic field lines in the presence of background inhomogeneities of the plasma, we are able to demonstrate the finite-β stabilization of drift waves and ion temperature gradient modes using a simple gyrokinetic particle code based on realistic fusion plasma parameters. However, for $\beta m_i/m_e \gg 1$, it becomes necessary to use the electron skin-depth as the grid size of the simulation to achieve accuracy in solving the resulting equations, unless special numerical arrangement is made for the cancelling of the two large terms on the either side of the governing equation. The proposed scheme is most suitable for studying shear-Alfvén physics in general geometry using straight field line coordinates for microturbulence and magnetic reconnection problems.

I. INTRODUCTION

The development of numerical schemes for solving finite-β gyrokinetic equations [1] for simulating shear-Alféven waves using a gyrokinetic particle code has a long history. It all started with two Ph.D. theses at Princeton University - first, the observation of the existence of streaming modes due to the fast electron motion above the Alfvén phase velocity [2] and, subsequently, the necessity of using a grid size of the electron skin-depth for the simulation [3], when the plasma β is above the mass ratio between the electrons and the ions, m_e/m_i. The problem of streaming modes was later resolved by the use of the finite-β split-weight scheme [4] based on the generalization of electrostatic perturbative methods [5, 6], where the response of the fast electrons is approximately assumed to be Boltzmann-like, i.e., adiabatic. In the present paper, we will present

a new finite-β split-weight scheme, which uses the double-split scheme, by taking out the additional adiabatic response of the fast particles to the field-line bending terms associated with the background inhomogeneity. Furthermore, we will show the resolution for the numerical difficulty facing us for high-β simulations for $\beta \gg m_e/m_i$. The term, arising from the electron inertia associated with the skin-depth term in the gyrokinetic Ampere's law [1], is thought to be important only for the cold electron response near the rational surfaces. However, we have found that the electron skin-depth, δ_e, which for $\beta \gg m_e/m_i$ is much smaller than the ion gyroradius, ρ_i, gives rise to the singular nature of the gyrokinetic Ampere's law and, as such, a grid spacing of the size of δ_e is actually need to be used as the grid size in the simulation domain to achieve accuracy in agreement with the earlier observation [3]. This is somewhat surprising, since one would think that δ_e is only important near the rational surface when magnetic tearing takes place. But, the singular nature of our equation, where the highest derivative term in the equation is multiplied by a smallness parameter [7, 8] calls for such a remedy, which we will explain. We will also show that this observation is consistent with the prevailing wisdom that the difficulty in simulating shear-Alfvén waves, when the plasma β is larger than the mass ratio, is due to the cancellation problem between the above-mentioned electron skin term and the warm electron source in the gyrokinetic Ampere's law [9–11], and the use of the electron skin-depth as the grid size in the simulation may be utilized to circumvent the cancellation problem. However, in the case when resolving the electron skin-depth is not desired (for example away from the rational surfaces), we will show how to modify the field equations to ensure that the cancellation happens numerically. We will also illustrate the relation of our approach to the hybrid approach of Lin & Chen [12].

The paper is organized as follows. In Sec. II, the governing finite-β gyrokinetic equations in the limit of $k_\perp \rho_i \ll 1$ are presented. In sec. III, a generalized split-weight numerical scheme including background inhomogeneity is discussed. The double split-weight scheme in simple geometry is the topic for Sec. IV. The theoretical properties of shear-Alfvén waves, drift instabilities and ion temperature gradient (ITG) modes are reviewed and the simulation results of finite-β modified microinstabilities are given in Sec. V. Finally, conclusions are drawn in Sec. IV. The ultimate goal of this study is the inclusion of finite-β effects in the global gyrokinetic particles codes such as GTC [13] and GTS [14]. Its purpose is not only for understanding the electromagnetic effects on micronistabilities, but is also a natural way to study the coupling between microturbulence and MHD in global toroidal geometry using the Particle-In-Cell (PIC) approach as described earlier [15]. This endeavour is intended as the continuation of the electromagnetic code development

effort of the present gyrokinetic codes, GEM [16] and GTC [17].

II. BASIC FORMULATION FOR FINITE-β PLASMAS

In the gyrokinetic units of $\rho_s (\equiv \sqrt{\tau}\rho_i)$ and Ω_i^{-1} for length and time, where $\Omega_i = eB_0/m_i c$ is the ion cyclotron frequency, $\rho_i = (T_i/m_i)^{1/2}/\Omega_i$ is the ion gyroradius, the governing gyrokinetic Vlasov equation for a finite-β plasma in the limit of $k_\perp^2 \rho_i^2 \ll 1$, can be written as [4, 15]

$$\frac{dF_\alpha}{dt} \equiv \frac{\partial F_\alpha}{\partial t} + v_\parallel \mathbf{b} \cdot \frac{\partial F_\alpha}{\partial \mathbf{x}} + \mathbf{E}^L \times \mathbf{b}_0 \cdot \frac{\partial F_\alpha}{\partial \mathbf{x}} + s_\alpha v_{t\alpha}^2 (\mathbf{E}^L \cdot \mathbf{b} + E_\parallel^T) \frac{\partial F_\alpha}{\partial v_\parallel} = 0, \qquad (1)$$

where $\tau \equiv T_e/T_i$ is the ratio of the electron, T_e, and the ion temperature, T_i, $\alpha \equiv e, i$ denotes species, $v_{te}^2 = m_i/m_e$, $v_{ti}^2 = 1/\tau$, $s_e = -1$, $s_i = \tau$,

$$\mathbf{b} \equiv \hat{\mathbf{b}}_0 + \frac{\delta \mathbf{B}}{B_0} = \frac{\mathbf{B_0}}{B_0} + \nabla A_\parallel \times \hat{\mathbf{b}}_0, \qquad (2)$$

$$\mathbf{E}^L = -\nabla \phi, \qquad E_\parallel^T = -\frac{\partial A_\parallel}{\partial t}, \qquad (3)$$

the superscripts L(longitudinal) and T(transverse) denote the vector decomposition relative to the direction of wave propagation and the subscript $\parallel$ indicates the direction parallel to the external magnetic field $\mathbf{B}_0$. The gyrokinetic Poisson's equation for $k_\perp^2 \rho_i^2 \ll 1$ can be simplified as

$$\nabla_\perp^2 \phi = - \int (F_i - F_e) dv_\parallel d\mu, \qquad (4)$$

where the electrostatic potential ϕ is normalized by T_e/e, $\int F_{0\alpha} dv_\parallel d\mu = 1$ and $\mu \equiv v_\perp^2/2$. Ampere's law then becomes

$$\nabla^2 A_\parallel = -\beta \int v_\parallel (F_i - F_e) dv_\parallel d\mu, \qquad (5)$$

where the vector potential $A_\parallel$ is normalized by cT_e/ec_s, $\beta \equiv c_s^2/v_A^2$, $v_A \equiv c\lambda_D/\rho_s$ is the Alfvén speed, $\lambda_D = (T_e/4\pi e^2 n_0)^{1/2}$ is the (unnormalized) electron Debye length, c is the speed of light and n_0 is the plasma density. [Note that the ion acoustic speed $c_s (\equiv \rho_s \Omega_i)$ is unity in the gyrokinetic unit.]

Equations (1) - (5) are the so-called electromagnetic Darwin model. The energy conservation of the resulting system of equations can be expressed as

$$\frac{1}{2}\frac{d}{dt}\left\langle \int \frac{v_\parallel^2 + v_\perp^2}{v_{te}^2} F_e dv_\parallel d\mu + \int \frac{v_\parallel^2 + v_\perp^2}{\tau v_{ti}^2} F_i dv_\parallel d\mu + |\nabla_\perp \phi|^2 + \frac{1}{\beta}|\nabla A_\parallel|^2 \right\rangle = 0, \qquad (6)$$

where $< \cdots >$ is the spatial average. Here, for our present purpose, we also assume the conservation of the magnetic moment for each particle,

$$\mu_B \equiv v_\perp^2/2B_0 \approx const. \tag{7}$$

This is a quasineutral system without the space charge waves where the normal mode frequencies in a homogeneous plasma are given by [4]

$$\omega^2 = k_\parallel^2 v_A^2/(1 + k^2 \delta_e^2) \tag{8}$$

and

$$\omega^2 = k_\parallel^2 v_A^2 (1 + k_\perp^2) \tag{9}$$

for cold and warm electron response, respectively, where

$$\delta_e = c/\omega_{pe} = \rho_s \left(\frac{m_e}{m_i \beta}\right)^{1/2} \tag{10}$$

is the electron skin-depth and $\omega_{pe} = v_{te}/\lambda_D$ is electron plasma frequency. The frequencies of Eq. (8) may set the limit for the time step of the simulation for low $\beta < m_e/m_i$ cases. By setting $A_\parallel = 0$, one recovers the electrostatic gyrokinetic Vlasov-Poisson system [18] and the associated numerical properties [19].

The scheme presented in the present paper is a generalization of the original split-weight scheme [4] by including the background inhomogeneities. It is suitable for finite-β simulations of tokamak plasmas using straight field lines coordinates. We can first re-write Eq. (1) as

$$\frac{dF_\alpha}{dt} \equiv \frac{\partial F_\alpha}{\partial t} + \left[v_\parallel \hat{\mathbf{b}}_0 - \nabla(\phi - v_\parallel A_\parallel) \times \hat{\mathbf{b}}_0\right] \cdot \frac{\partial F_\alpha}{\partial \mathbf{x}}$$
$$- s_\alpha v_{t\alpha}^2 (\nabla\psi + \nabla\phi \times \nabla A_\parallel) \cdot \hat{\mathbf{b}}_0 \frac{\partial F_\alpha}{\partial v_\parallel} = 0, \tag{11}$$

where

$$\hat{\mathbf{b}}_0 \cdot \nabla\psi \equiv \hat{\mathbf{b}}_0 \cdot \nabla\phi + \frac{\partial A_\parallel}{\partial t}. \tag{12}$$

This governing gyrokinetic equation takes the phase space conservation form of

$$\frac{\partial F_\alpha}{\partial t} + \frac{\partial}{\partial \mathbf{x}} \cdot \left(\frac{d\mathbf{x}}{dt} F_\alpha\right) + \frac{\partial}{\partial v_\parallel} \left(\frac{dv_\parallel}{dt} F_\alpha\right) = 0 \tag{13}$$

with

$$\frac{d\mathbf{x}}{dt} = v_\parallel \hat{\mathbf{b}}_0 - \nabla(\phi - v_\parallel A_\parallel) \times \hat{\mathbf{b}}_0, \tag{14}$$

and

$$\frac{dv_\parallel}{dt} = -s_\alpha v_{t\alpha}^2 (\nabla\psi + \nabla\phi \times \nabla A_\parallel) \cdot \hat{\mathbf{b}}_0. \tag{15}$$

Equations (13) - (15) along with the Klimontovich-Dupree representation for particle distribution function

$$F_\alpha(\mathbf{x}, v_\parallel, t) = \sum_{j=1}^{N} \delta(\mathbf{x} - \mathbf{x}_{\alpha j}) \delta(\mu - \mu_{\alpha j}) \delta(v_\parallel - v_{\alpha\parallel j}), \tag{16}$$

where N is the total number of simulation particles, are the focus of the present paper. This complete set of equations are amenable for particle pushing because of its conservation properties [19].

III.   THE PERTURBATIVE SIMULATION SCHEMES

Let us first cast Eq. (13) into the δf formalism. Namely, for $F_\alpha = F_{0\alpha} + \delta f_\alpha$ and $\partial F_{0\alpha}/\partial t + v_\parallel \hat{\mathbf{b}}_0 \cdot \partial F_{0\alpha}/\partial \mathbf{x} = 0$, we obtain

$$\frac{d\delta f_\alpha}{dt} = -\nabla(\phi - v_\parallel A_\parallel) \times \hat{\mathbf{b}}_0 \cdot \boldsymbol{\kappa}_\alpha F_{0\alpha} - s_\alpha v_\parallel (\nabla\psi + \nabla\phi \times \nabla A_\parallel) \cdot \hat{\mathbf{b}}_0 F_{0\alpha}, \tag{17}$$

and, for $w_\alpha \equiv \delta f_\alpha/F_\alpha$, the weight equation now becomes

$$\frac{dw_\alpha}{dt} = -(1 - w_\alpha)\frac{1}{F_{0\alpha}}\frac{d\delta f_\alpha}{dt}, \tag{18}$$

where $\boldsymbol{\kappa}_\alpha \equiv -(\partial F_{0\alpha}/\partial\mathbf{x})/F_{0\alpha} = \boldsymbol{\kappa}_n - \frac{3}{2}\boldsymbol{\kappa}_{T\alpha} + \frac{1}{2}\boldsymbol{\kappa}_{T\alpha}(v_\parallel^2 + v_\perp^2)/v_{t\alpha}^2$, $\boldsymbol{\kappa}_n \equiv -dlnn_0/d\mathbf{x}$, and $\boldsymbol{\kappa}_{T\alpha} \equiv -dlnT_{0\alpha}/d\mathbf{x}$ represent the zeroth-order inhomogeneities and $F_{0\alpha} \equiv (1/\sqrt{2\pi}v_{t\alpha}^3)exp[-(v_\parallel^2 + v_\perp^2)/2v_{t\alpha}^2]$ is the background Maxwellian. The field equations become

$$\nabla_\perp^2 \phi = -\int (\delta f_i - \delta f_e)dv_\parallel d\mu, \tag{19}$$

and

$$\nabla^2 A_\parallel = -\beta \int v_\parallel(\delta f_i - \delta f_e)dv_\parallel d\mu. \tag{20}$$

This is the familiar δf scheme [6], and

$$\delta f_\alpha(\mathbf{x}, v_\parallel, t) = \sum_{j=1}^{N} w_{\alpha j}\delta(\mathbf{x} - \mathbf{x}_{\alpha j})\delta(\mu - \mu_{\alpha j})\delta(v_\parallel - v_{\parallel\alpha j}). \tag{21}$$

As we know, δf scheme has numerical difficulties in simulating shear-Alfvén waves [4] without further separating the adiabatic response from δf by using the split-weight scheme [5]. In the present paper, we will first describe the generalization of the split-weight scheme used earlier

by Lee *et al.* [4] for solving ψ in a shearless slab geometry defined in Eq. (12), by including background inhomogeneity. For $F_\alpha = F_{0\alpha} + \delta f_\alpha = e^{-s_\alpha \psi} F_{0\alpha} + \delta h_\alpha$, for which $\delta f_\alpha \approx -s_\alpha \psi F_{0\alpha} + \delta h_\alpha$. The evolution for the nonadiabtic response part of the perturbed distribution becomes

$$\frac{d\delta h_\alpha}{dt} = e^{-s_\alpha \psi} F_{0\alpha} \left[s_\alpha \frac{\partial \psi}{\partial t} - \nabla(\phi - v_\parallel A_\parallel) \times \hat{\mathbf{b}}_0 \cdot (\boldsymbol{\kappa}_\alpha + s_\alpha \nabla \psi) - s_\alpha v_\parallel \nabla \phi \times \nabla A_\parallel \cdot \hat{\mathbf{b}}_0 \right] \quad (22)$$

For $w_\alpha^{NA} \equiv \delta h_\alpha / F_\alpha$, the corresponding weight is

$$\frac{dw_\alpha^{NA}}{dt} = (1 - w_\alpha^{NA}) \frac{1}{F_{0\alpha}} \frac{d\delta h_\alpha}{dt}. \quad (23)$$

For a scheme using δh_e and δh_i, with $k_\parallel \ll k_\perp$, the corresponding field equations for ϕ and $A_\parallel$ are

$$\nabla_\perp^2 \phi - (1 + \tau)\psi = -\int (\delta h_i - \delta h_e) dv_\parallel d\mu, \quad (24)$$

and

$$\nabla_\perp^2 A_\parallel = -\beta \int v_\parallel (\delta h_i - \delta h_e) dv_\parallel d\mu, \quad (25)$$

respectively. Taking $\partial/\partial t$ of Eqs. (24) and (25), and substituting $\partial \delta h_i / \partial t$ and $\partial \delta h_e / \partial t$ from Eq. (22), respectively, we arrive at

$$\nabla_\perp^2 \frac{\partial \phi}{\partial t} = \hat{\mathbf{b}}_0 \cdot \nabla \int v_\parallel (\delta h_i - \delta h_e) dv_\parallel d\mu, \quad (26)$$

$$\nabla_\perp^2 \frac{\partial A_\parallel}{\partial t} = \beta \left[\hat{\mathbf{b}}_0 \cdot \nabla \int v_\parallel^2 (\delta h_i - \delta h_e) dv_\parallel d\mu + \nabla A_\parallel \times \hat{\mathbf{b}}_0 \cdot [v_{te}^2 (\boldsymbol{\kappa}_n + \boldsymbol{\kappa}_{Te}) - v_{ti}^2 (\boldsymbol{\kappa}_n + \boldsymbol{\kappa}_{Ti})] \right], \quad (27)$$

where nonlinear terms have been ignored (see, Eq. (17) in Ref. [5]). Again taking $\partial/\partial t$ of Eq. (27) and substituting the resulting time derivatives for δh_i and δh_e by the proper equations, we obtain

$$(\nabla_\perp^2 - \beta v_{te}^2 - \beta) \frac{\partial^2 A_\parallel}{\partial t^2} = \beta \left[- (\hat{\mathbf{b}}_0 \cdot \nabla)^2 \int v_\parallel^3 (\delta h_i - \delta h_e) dv_\parallel d\mu \right.$$

$$\left. + (v_{te}^2 + 1)\hat{\mathbf{b}}_0 \cdot \nabla \frac{\partial \phi}{\partial t} + \hat{\mathbf{b}}_0 \cdot \nabla(\nabla \psi \times \hat{\mathbf{b}}_0) \cdot [v_{te}^2 (\boldsymbol{\kappa}_n + \boldsymbol{\kappa}_{Te}) - v_{ti}^2 (\boldsymbol{\kappa}_n + \boldsymbol{\kappa}_{Ti})] \right], \quad (28)$$

where $\hat{\mathbf{b}}_0 \cdot \nabla(\nabla \phi \times \hat{\mathbf{b}}_0) + \nabla(\partial A_\parallel / \partial t) \times \hat{\mathbf{b}}_0 = \hat{\mathbf{b}}_0 \cdot \nabla(\nabla \psi \times \hat{\mathbf{b}}_0)$ is used.

Thus, particle pushing can be carried out with Eqs. (14) and (15), along with Eq. (23) for the non-adiabatic part of particle weights. Equations (24) - (28) are the five field equations for ϕ, $A_\parallel$, $\partial \phi / \partial t$, $\partial A_\parallel / \partial t$, and $\partial^2 A_\parallel / \partial t^2$, respectively, where

$$\delta h_\alpha = \sum_{j=1}^N w_{\alpha j}^{NA} \delta(\mathbf{x} - \mathbf{x}_{\alpha j}) \delta(\mu - \mu_{\alpha j}) \delta(v_\parallel - v_{\parallel \alpha j}) \quad (29)$$

and N is the number of particles. The field quantity ψ is given by Eq. (12), i.e.,

$$\psi = \phi + \int \frac{\partial A_\parallel}{\partial t} dx_{\parallel 0}, \tag{30}$$

and its time derivative, $\partial\psi/\partial t$, can be calculated accordingly from $\partial\phi/\partial t$ and $\partial^2 A_\parallel/\partial t^2$.

Alternatively, in the limit where $(\hat{\mathbf{b}}_0 \cdot \nabla)\nabla_\perp^2 \phi = \nabla_\perp^2(\hat{\mathbf{b}}_0 \cdot \nabla\phi)$, and using Eqs. (12) and (24), Eq. (27) can be simplified as

$$(\nabla_\perp^2 - 1 - \tau)(\hat{\mathbf{b}}_0 \cdot \nabla\psi) = \beta(\hat{\mathbf{b}}_0 \cdot \nabla)\int v_\parallel^2(\delta h_i - \delta h_e)d\mu dv_\parallel - (\hat{\mathbf{b}}_0 \cdot \nabla)\int(\delta h_i - \delta h_e)d\mu dv_\parallel$$
$$+ \beta\nabla A_\parallel \times \hat{\mathbf{b}}_0 \cdot \left[\frac{m_i}{m_e}(\boldsymbol{\kappa}_n + \boldsymbol{\kappa}_{Te}) - \frac{1}{\tau}(\boldsymbol{\kappa}_n + \boldsymbol{\kappa}_{Ti})\right]. \tag{31}$$

Similarly, we can also simply Eqs. (26) and (28) to

$$[\nabla_\perp^2 - \beta\frac{m_i}{m_e} - \beta]\frac{\partial\psi}{\partial t} = -\beta(\hat{\mathbf{b}}_0 \cdot \nabla)\int v_\parallel^3(\delta h_i - \delta h_e)d\mu dv_\parallel + (\hat{\mathbf{b}}_0 \cdot \nabla)\int v_\parallel(\delta h_i - \delta h_e)d\mu dv_\parallel$$
$$+ \beta\nabla\psi \times \hat{\mathbf{b}}_0 \cdot \left[\frac{m_i}{m_e}(\boldsymbol{\kappa}_n + \boldsymbol{\kappa}_{Te}) - \frac{1}{\tau}(\boldsymbol{\kappa}_n + \boldsymbol{\kappa}_{Ti})\right]. \tag{32}$$

The former can be considered as a generalized Ohm's law, while the latter a kind of vorticity equation. So, in this limit, the governing field equations are reduced to Eqs. (24), (25), (31), and (32), and Eqs. (23) and (29) describe the time evolution of the perturbed distribution.

We should remark here that these equations, without the inhomogeneity terms, are similar to those used for the study of shear-Alfvén waves earlier, where the original split-weight scheme for finite-β plasmas [4] was devised. However, we found that the original split-weight scheme had stability problems when density gradients were included in the simulation and the solution for which is the topic for the remaining of this paper.

Finally, let us point out that the linearized Eqs. (25), (26) and (28) can also be simplified to the two-field MHD equations [20], i.e.,

$$\nabla_\perp^2 \frac{\partial\phi}{\partial t} + \frac{1}{\beta}\hat{\mathbf{b}}_0 \cdot \nabla\nabla_\perp^2 A_\parallel = 0, \tag{33}$$

and

$$\frac{\partial A_\parallel}{\partial t} + \hat{\mathbf{b}}_0 \cdot \nabla\phi = 0. \tag{34}$$

in the limit of cold ion and electrons with $(ck_\perp/\omega_{pe})^2[\equiv (k_\perp\rho_s)^2(m_e/m_i\beta)] \ll 1$. They are the vorticity equation and the parallel collisionless Ohm's law, respectively. These reduced two-field MHD equations give rise to the usual shear-Alfvén waves of $\omega = \pm k_\parallel v_A$ in the zero electron mass limit.

IV.   THE DOUBLE SPLIT-WEIGHT SCHEME

The numerical difficulty associated with the original split-weight scheme [4] comes from the fact that the resulting weight equation, Eq. (23), contains $v_\parallel$ terms, i.e., those associated with the presence of $A_\parallel$, which, for accuracy purposes, need small time steps in the simulation to resolve. Thus, the existing split-weight schemes [4, 5], designed for eliminating $v_\parallel$ terms, are not sufficient when the finite-β effects, through $v_\parallel A_\parallel$ terms, are included in the simulation. To circumvent the problem, let us present a new scheme, as first pointed out in 2007 [21], by further separating out the fast particle response to the quasi-static bending of the magnetic field lines as

$$F_\alpha = F_{0\alpha} e^{-s_\alpha \psi} + F_{0\alpha} e^{-s_\alpha \psi} \int dx_\parallel \boldsymbol{\kappa}_\alpha \cdot (\nabla A_\parallel \times \hat{\mathbf{b}}_0) + \delta g_\alpha, \tag{35}$$

for both the electrons and the ions, so that a new full inhomogeneous gradient, background plus perturbation, which is set up by the fast particles, is transverse to the direction of the field, background plus perturbation, i.e.,

$$\mathbf{b} \cdot \nabla \left[1 + \int dx_\parallel \boldsymbol{\kappa}_\alpha \cdot (\nabla A_\parallel \times \hat{\mathbf{b}}_0) \right] F_{0\alpha} e^{-s_\alpha \psi} \approx 0, \tag{36}$$

where $\mathbf{b} = \hat{\mathbf{b}}_0 + \delta\mathbf{B}/B_0$. (An independent, but more general, idea of separating out the background magnetic field in toroidal geometry was given Nishimura et al. in 2007 [22])

The evolution for the remaining linear response for the particles, from Eq. (22), becomes

$$\frac{d\delta g_\alpha}{dt} = \left[s_\alpha \frac{\partial \psi}{\partial t} - \nabla\psi \times \hat{\mathbf{b}}_0 \cdot \boldsymbol{\kappa}_\alpha \right] F_{0\alpha} e^{-s_\alpha \psi}, \tag{37}$$

where the disappearance of the explicitly $v_\parallel$ dependent term associated the spatial inhomogeneity, unlike those in Eqs. (22) and (23), gives us the numerical advantage. Let $w_\alpha^{DNA} \equiv \delta g_\alpha / F_\alpha$, the corresponding time evolution for the particle weight of species α takes the form of

$$\frac{dw_\alpha^{DNA}}{dt} = (1 - w_\alpha^{DNA}) \left[s_\alpha \frac{\partial \psi}{\partial t} - \nabla\psi \times \hat{\mathbf{b}}_0 \cdot \boldsymbol{\kappa}_\alpha \right], \tag{38}$$

by assuming that $|\int dx_\parallel \boldsymbol{\kappa}_\alpha \cdot (\nabla A_\parallel \times \hat{\mathbf{b}}_0)| \ll 1$, which, in turn, gives

$$\delta g_\alpha = \sum_{j=1}^{N} w_{\alpha j}^{DNA} \delta(\mathbf{x} - \mathbf{x}_{\alpha j}) \delta(\mu - \mu_{\alpha j}) \delta(v_\parallel - v_{\parallel \alpha j}) \tag{39}$$

and N is the total number of particles in the simulation. While Eqs. (14) and (15) for particle advance remain the same for the new scheme, the governing field equations of Eqs. (24)-(28) then become

$$\nabla_\perp^2 \phi - (1 + \tau)\psi = -\int (\delta g_i - \delta g_e) dv_\parallel d\mu, \tag{40}$$

$$\nabla_\perp^2 A_\| = -\beta \int v_\|(\delta g_i - \delta g_e)dv_\| d\mu, \tag{41}$$

$$\nabla_\perp^2 \frac{\partial \phi}{\partial t} = \hat{\mathbf{b}}_0 \cdot \nabla \int v_\|(\delta g_i - \delta g_e)dv_\| d\mu, \tag{42}$$

$$\nabla_\perp^2 \frac{\partial A_\|}{\partial t} = \beta \hat{\mathbf{b}}_0 \cdot \nabla \int v_\|^2(\delta g_i - \delta g_e)dv_\| d\mu, \tag{43}$$

for $e^{-s_\alpha \psi} \approx 1$ and

$$(\nabla_\perp^2 - \beta v_{te}^2 - \beta)\frac{\partial^2 A_\|}{\partial t^2} = \beta\Bigg[- (\hat{\mathbf{b}}_0 \cdot \nabla)^2 \int v_\|^3(\delta g_i - \delta g_e)dv_\| d\mu$$

$$+(v_{te}^2 + 1)\hat{\mathbf{b}}_0 \cdot \nabla \frac{\partial \phi}{\partial t} + \hat{\mathbf{b}}_0 \cdot \nabla(\nabla\psi \times \hat{\mathbf{b}}_0) \cdot [v_{te}^2(\boldsymbol{\kappa}_n + \boldsymbol{\kappa}_{Te}) - v_{ti}^2(\boldsymbol{\kappa}_n + \boldsymbol{\kappa}_{Ti})]\Bigg], \tag{44}$$

respectively, while Eqs. (31) and (32) in terms of δg_α take the form of

$$(\nabla_\perp^2 - 1 - \tau)\psi = \beta \int v_\|^2(\delta g_i - \delta g_e)d\mu dv_\| - \int (\delta g_i - \delta g_e)d\mu dv_\|, \tag{45}$$

for $e^{-s_\alpha \psi} \approx 1$ and

$$[\nabla_\perp^2 - \beta\frac{m_i}{m_e} - \beta]\frac{\partial \psi}{\partial t} = -\beta(\hat{\mathbf{b}}_0 \cdot \nabla) \int v_\|^3(\delta g_i - \delta g_e)d\mu dv_\| + (\hat{\mathbf{b}}_0 \cdot \nabla) \int v_\|(\delta g_i - \delta g_e)d\mu dv_\|$$

$$+\beta\nabla\psi \times \hat{\mathbf{b}}_0 \cdot \left[\frac{m_i}{m_e}(\boldsymbol{\kappa}_n + \boldsymbol{\kappa}_{Te}) - \frac{1}{\tau}(\boldsymbol{\kappa}_n + \boldsymbol{\kappa}_{Ti})\right], \tag{46}$$

respectively. Equations (37) - (46) represent the full system of equations for simulating gyrokinetic plasmas with finite β. Note that ψ and $\partial\psi/\partial t$ can be calculated either by using Eq. (12), i.e., $\psi = \phi + \int(\partial A_\|/\partial t)dx_{\|0}$, from Eqs. (40), (42), (43) and (44), or by using Eqs. (45) and (46), directly. From Eq. (40), Eq. (45) can also be expressed as

$$\nabla_\perp^2(\psi - \phi) = \beta \int v_\|^2(\delta g_i - \delta g_e)d\mu dv_\| \tag{47}$$

based on the double split-weight scheme. Similarly, Eq. (46) can be expressed in terms of Eq. (42) as well via its integral in $v_\|$.

V. THEORY AND SIMULATION OF FINITE-β STABILIZATION OF MICROINSTABILITIES

In the present work, the gyrokinetic Vlasov equation, Eq. (37), and the associated field equations, Eqs. (45) and (46), have been used as a complete set of equations describing the self-consistent evolution of fields and particles. In this section we will describe the numerical properties

and the numerical methods used to solve these equations and the comparisons between the simulation results and the theoretical predictions on the linear properties of the shear-Alfvén and finite-β modified microinstabilities.

Let us first point out a interesting aspect of Eq. (46). Namely, it can be symbolically written as

$$\left(\nabla_\perp^2 - \frac{1}{\delta_e^2}\right) y = G, \tag{48}$$

where δ_e is the electron skin-depth normalized by ρ_s as given by Eq. (10), which can be much smaller than unity for high β plasmas, and G represents the contents of the RHS of Eq. (46). Multiplying Eq. (48) by δ_e^2, it then takes the form of a singularly perturbed equation, where the highest derivative is multiplied by a smallness parameter, in which the three terms represent diffusion, source and driving, respectively, using the terms commonly adopted in the literature [7, 8]. As such, the scale-length prescribed by Eq. (48) as well as Eq. (46) can be normalized by the electron skin-depth - a fundamental quantity of our system. From our governing electromagnetic equations, Eqs. (46) and (10) in the limit of the cold electrons ($\omega/k_\parallel \gg v_{te}$) and ions ($\omega/k_\parallel \gg v_{ti}$) for a homogeneous plasma, using the the ansatz of $exp(-i\omega t + i\mathbf{k} \cdot \mathbf{x})$, we can write the dispersion relation approximately in the integral form of

$$D\left(\frac{\lambda_D^2}{\rho_s^2}\right) \equiv 1 + \omega_A^2 \int_0^\infty t exp(-i\omega t - \frac{1}{2}k_\parallel^2 v_{te}^2 t^2)dt = 0, \tag{49}$$

where ω is the complex frequency, $\mathbf{k}$ is the wave vector, and

$$\omega_A^2 \equiv k_\parallel^2 v_A^2/(1 + k_\perp^2 \delta_e^2) = \omega_H^2/(1 + 1/k_\perp^2 \delta_e^2) \tag{50}$$

are the normal modes of the system for $\beta < m_e/m_i$. They are the inertial Alfven waves, with the denominator coming from the first two terms on the LHS of Eq. (46). Following the same arguments used by Langdon based on ω_{pe} and λ_D for an unmagnetized plasma [23, 24] as well as by Lee based on ω_H and ρ_s for a gyrokinetic plasma [19], we may conclude from Eq. (49) that it gives us the time step and grid spacing restrictions of $\omega_A \Delta t \leq 1$ and $\Delta x \leq \delta_e$ similar to the roles of $\omega_{pe}\Delta t \leq 1$ and $\Delta x \leq \lambda_D$ [23, 24] for unmagnetized plasma and $\omega_H \Delta t \leq 1$ and $\Delta x \leq \rho_s$ for an electrostatic gyrokinetic plasma [19]. In all these cases, $k_\parallel v_{te}\Delta t \leq 1$ is required for accuracy purposes. However, in the high β limit, i.e., $\beta m_i/m_e \gg 1$, when $\delta_e \ll \rho_s$ and the electron response is warm, the normal modes become [4]

$$\omega_A^2 \equiv k_\parallel^2 v_A^2 (1 + k_\perp^2), \tag{51}$$

where the electron skin depth does not play a role. One would assume that we can use a grid of the size of $\rho_s \gg \delta_e$. However, as Cummings [3] has pointed out, that a numerical grid of $\Delta x \approx \delta_e \ll \rho_s$ is indeed needed regardless the plasma β. This puzzling observation has also been verified by us by solving Eqs. (37), (45) and (46). One possible way to understand this is to write Eq. (48) in the finite difference form, i.e.,

$$\frac{\delta_e^2}{\Delta x^2} \left[y(\mathbf{x} + \Delta \mathbf{x}) - 2y(\mathbf{x}) + y(\mathbf{x} - \Delta \mathbf{x}) \right] - y(\mathbf{x}) = \delta_e^2 G(\mathbf{x}), \tag{52}$$

where $\Delta \mathbf{x}$ is the grid size. Thus, for $\delta_e \ll \Delta x$, we may run into accuracy problems for the reasons that Eqs. (48) and (52) may support either highly oscillatory or tearing-type solutions. This observation may be related to the stringent grid size requirement discussed in Refs. [7, 8] for singularly perturbed equations. For us, this accuracy problem is perhaps further exacerbated by the presence of the third order velocity moments in Eq.(46).

However, this restriction on the grid size can be removed if one deals with Eqs. (45) and (46) based on physical arguments as follows. Let us re-write Eq. (46) symbolically as

$$\left(\frac{d^2}{dx^2} + \frac{1}{\delta_e^2} \right) y = \frac{1}{\delta_e^2} F(y) + G(y). \tag{53}$$

Here, $F(y)/\delta_e^2$ represents the electron contribution to the right-hand side in Eq. (46) and $G(y)$ is the remaining contributions due to the ions as well as the electrons. There are two different type of modes that are described by Eqs. (46) or (53), slow modes with $\omega/k_\parallel \ll v_{te}$ for which electron response is warm and nearly adiabatic, and fast modes with $\omega/k_\parallel \geq v_{te}$ for which the response is cold and non-adiabatic. For the latter case, it can be easily seen from Eq. (37) that the first term on the RHS of Eq. (53) is negligible and we need a grid of the size of δ_e.

On the other hand, for slow modes with $\omega/k_\parallel \ll v_{te}$, it can be easily seen from Eq. (37) that the function F has a form $F(y) = y + \delta_e^2 \tilde{F}(y)$, with first term due to the nearly adiabatic response of the electrons. For these waves the large terms in Eq. (53) proportional to $1/\delta_e^2$ cancel and the resulting equation has a form

$$\frac{d^2}{dx^2} y = \tilde{F}(y) + G(y), \tag{54}$$

which contains no large parameter $1/\delta_e^2$ and therefore does not require any special care to find its solution numerically. What is required in this case is the accurate calculation of large terms in adiabatic electron response [the term y in expression $F(y) = y + \delta_e^2 \tilde{F}(y)$] which should cancel equally large term on the left hand side of Eqs.(53) or Eq. (46). As shown in Appendix A,

because of the finite grid size approximation in calculating the electron response, the numerical approximation to function $F(y)$ has a form

$$F(y) = \left(1 + \frac{1}{6}\Delta x^2 \frac{d^2}{dx^2}\right)y + \delta_e^2 \tilde{F}(y). \tag{55}$$

Substitution of Eq. (55) into Eq. (53) produces the equation

$$\left(1 - \frac{1}{6}\frac{\Delta x^2}{\delta_e^2}\right)\frac{d^2}{dx^2}y = \tilde{F}(y) + G(y). \tag{56}$$

Comparing it with Eq. (54), the solution of Eq. (56) will correctly approximate the solution of Eq. (54) if the grid size is sufficiently small $\Delta x \ll \delta_e$, i.e., the if the electron skin-depth is resolved. Note that resolving the electron skin-depth for modes with $\omega/k_\| \ll v_{te}$ is needed to accurately cancel large terms in original Eq. (53) or (46) and therefore is necessary for modes with arbitrary transverse wavelength, even the ones with $\lambda_\perp \gg \delta_e$.

To avoid resolving the electron skin-depth for these slow modes with $\lambda_\perp \gg \delta_e$ we can modify the left-hand side of Eq. (46) and (53) as described in Appendix A, which insures accurate cancellation of the large terms even when the skin-depth is not resolved. This corresponds to replacing large parameters $1/\delta_e^2$ in Eq. (53) with differential operator $1/\delta_e^2 \rightarrow (1/\delta_e^2)(1 + [\Delta x^2/6]d^2/dx^2)$, and similarly, the introduction of operator A in Eq. (46) as follows,

$$[\nabla_\perp^2 - A\beta\frac{m_i}{m_e} - \beta]\frac{\partial\psi}{\partial t} = -\beta(\hat{\mathbf{b}}_0 \cdot \nabla)\int v_\|^3(\delta g_i - \delta g_e)d\mu dv_\| + (\hat{\mathbf{b}}_0 \cdot \nabla)\int v_\|(\delta g_i - \delta g_e)d\mu dv_\| +$$
$$\beta\nabla\psi \times \hat{\mathbf{b}}_0 \cdot \left[A\frac{m_i}{m_e}(\boldsymbol{\kappa}_n + \boldsymbol{\kappa}_{Te}) - \frac{1}{\tau}(\boldsymbol{\kappa}_n + \boldsymbol{\kappa}_{Ti})\right], \tag{57}$$

where $A = \sum_{\mathbf{k}} A(\mathbf{k})exp(i\mathbf{k}\cdot\mathbf{x})$ and $A(\mathbf{k}) \approx 1 - (\mathbf{k}_\perp^2\Delta x_\perp^2 + k_\|^2\Delta x_\|^2)/6$ for $(\mathbf{k}_\perp^2\Delta x_\perp^2 + k_\|^2\Delta x_\|^2) \ll 1$. The derivation of Eq. (57) is given in Appendix A.

Note that, in the situations when both modes, fast with $\omega/k_\| \geq v_{te}$ and slow with $\omega/k_\| \ll v_{te}$ are present (for example in simulations around rational surface in tokomaks), resolving the electron skin-depth to numerically resolve the wavelength of short-wavelength modes with $\omega/k_\| \geq v_{te}$ also insures the cancellation of large terms for modes with adiabatic electron response for which $\omega/k_\| \ll v_{te}$.

In this paper we present results of linear simulations with periodic boundary conditions in transverse direction. Equation (46) is solved using Fast Fourier Transform (FFT) where short-wavelength modes are filtered out, and only long-wavelength modes with $\lambda_\perp \gg \delta_e$ are kept. Because only long-wavelength modes are kept, the "singular perturbed" property of field equation (46) did not present any problem, while cancellation problem was dealt with by using corrected field equation (57). That allowed us to use much coarser grid resolution $\lambda_\perp \gg \Delta x \gg \delta_e$.

In the future work where the magnetic tearing modes in sheared geometry will be studied, the electron skin-depth may need to be resolved to produce accurate numerical results.

Before presenting the simulation results, let us first describe the linear dispersion relation for the shear-Alfvén waves and the finite-β modified drift waves as follows. Using the ansatz of $\exp(i\mathbf{k}\cdot\mathbf{x} - i\omega t)$ with $\boldsymbol{\kappa}_i = \boldsymbol{\kappa}_e = \kappa_n\hat{\mathbf{y}}$ (in $\{y, x, z\}$ coordinate system), and $\omega_* = k_x\kappa_n$, the perturbed ion distribution for $k_\parallel v_\parallel \ll \omega$, from Eq. (17), can be written as

$$\delta f_i = \frac{\omega_*}{\omega}(\phi - v_\parallel A_\parallel)F_{0i} + \tau\frac{k_\parallel v_\parallel}{\omega}\psi F_{0i} \tag{58}$$

and the non-adiabatic electron distribution Eq. (22), for $\omega \ll k_\parallel v_\parallel$, becomes

$$\delta h_e = \left[\frac{\omega}{k_\parallel v_\parallel}\psi - \frac{\omega_*}{k_\parallel v_\parallel}(\phi - v_\parallel A_\parallel)\right](1 + \frac{\omega}{k_\parallel v_\parallel} + \frac{\omega^2}{k_\parallel^2 v_\parallel^2})F_{0e} + i\pi\delta(k_\parallel v_\parallel - \omega)[\omega\psi - \omega_*(\phi - v_\parallel A_\parallel)]F_{0e}. \tag{59}$$

Substituting them into Eqs. (24) and (25), and noting that $\psi = \phi - (\omega/k_\parallel)A_\parallel$, we can write the dispersion relation as

$$k_\perp^2 = \left(\frac{\omega_*}{\omega} - 1\right)\left(1 - \beta\frac{\omega^2}{k_\parallel^2}\right)\left(1 + i\sqrt{\frac{\pi}{2}}\frac{\omega}{k_\parallel v_{te}}\right) - \beta\left(1 + \frac{\omega_*}{\tau\omega}\right), \tag{60}$$

where $k_\perp^2 = k_x^2 + k_y^2$ and the last term on the RHS comes from the parallel ion dynamics. The same dispersion relation can also be obtained by using the generalized Ohm's law, Eq. (31). For $\omega_* = 0$, we recover the damped shear-Alfvén waves with

$$\omega_l = \pm k_\parallel v_A\sqrt{1 + k_\perp^2 + \beta}, \tag{61}$$

where $v_A = 1/\sqrt{\beta}$ and

$$\frac{\gamma_l}{\omega_l} = -\frac{1}{2}\sqrt{\frac{\pi}{2}}\frac{\omega_l}{k_\parallel v_{te}}\frac{k_\perp^2}{1 + k_\perp^2}. \tag{62}$$

For the finite-β modified drift waves, the linear frequencies and growth rates can be obtained approximately as

$$\frac{\omega_l}{\omega_*} = \frac{1}{1 + k_\perp'^2} \tag{63}$$

and

$$\frac{\gamma_l}{\omega_l} \approx \sqrt{\frac{\pi}{2}}\frac{\omega_l}{k_\parallel v_{te}}\frac{k_\perp'^2}{1 + k_\perp'^2}, \tag{64}$$

respectively, where

$$\begin{aligned}
k_\perp'^2 &= k_\perp^2 + \beta\left(\frac{\omega_*}{\omega_l} - 1\right)\frac{\omega_l^2}{k_\parallel^2} + \beta\left(1 + \frac{\omega_*}{\tau\omega_l}\right) \\
&\approx k_\perp^2 + \beta\left[\left(\frac{k_\perp}{k_\parallel}\right)^2\left(\frac{\omega_*}{1 + k_\perp^2}\right)^2 + \frac{1 + k_\perp^2}{\tau} + 1\right] \geq k_\perp^2
\end{aligned} \tag{65}$$

and Eq. (63) has been used. Thus, both the linear frequencies and the linear growth rates are lowered by the finite-β effects. Note that the finite-β contribution by the ions to the damping rate has been ignored in the present calculation. When $\beta = 0$, we then recover the electrostatic results, for example, as those given in Ref. [5]. A more complete version of the dispersion relation, than that of Eq. (60), by including the complete plasma response, can be written as

$$k_\perp^2 + (1 - \beta \frac{\omega^2}{k_\parallel^2}) \left[(1 - \frac{\omega_*}{\omega})(1 + X_e) + (\tau + \frac{\omega_*}{\omega})(1 + X_i) \right] = 0, \tag{66}$$

where $X_\alpha \equiv \xi_\alpha Z(\xi_\alpha)$, $\xi_\alpha \equiv \omega/\sqrt{2}k_\parallel v_{t\alpha}$ and Z is the usual plasma dispersion function. Similarly, for including the electron and ion temperature gradient (ETG & ITG) modes, the dispersion relation becomes

$$k_\perp^2 + (1 - \beta \frac{\omega^2}{k_\parallel^2}) \Bigg\{ (1 + X_e) + \tau(1 + X_i) - \frac{\omega_*}{\omega}(X_e - X_i)$$
$$+ \frac{\omega_{*Te}}{\omega} \left[\frac{X_e}{2} - \xi_e^2(1 + X_e) \right] - \frac{\omega_{*Ti}}{\omega} \left[\frac{X_i}{2} - \xi_i^2(1 + X_i) \right] \Bigg\} = 0, \tag{67}$$

where $\omega_{*T\alpha} \equiv k_x \kappa_{T\alpha}$. For the ITG modes only with $\omega_* = 0$ and $\omega_{*Te} = 0$, in the cold ion limit $(X_i \approx -1 - 1/2\xi_i^2 - 3/4\xi_i^4)$ together with adiabatic electrons $(X_e \approx 0)$, it can then be written as

$$k_\perp^2 + (1 - \beta \frac{\omega^2}{k_\parallel^2}) \left[1 - (\tau + \frac{\omega_{*Ti}}{\omega}) \frac{k_\parallel^2 v_{ti}^2}{\omega^2} \right] = 0. \tag{68}$$

In the limit of $\beta \to 0$ and $\tau \ll \omega_{*Ti}/\omega$, we recover the usual unstable electrostatic eigenmode from the resulting cubic equation as [25]

$$\frac{\omega}{\omega_{*Ti}} \approx \frac{-1 + i\sqrt{3}}{2} \left(\frac{k_\parallel v_{ti}}{\omega_{*Ti}} \right)^{2/3} \left(\frac{1}{1 + k_\perp^2} \right)^{1/3} \tag{69}$$

For $\beta \neq 0$, Eq. (68) becomes a fifth-order algebraic equation in (ω/ω_{*Ti}), and the corresponding growth rates show a slight increase as a function of β. The finite-β stabilization of ITG modes appears only if finite gyro-radius effects are included. The equations that include finite gyro-radius effects are derived in Appendix C.

To verify the validity of the proposed double split-weight scheme in Sec. IV in comparisons with the linear properties of finite-β modified microinstabilities described above, let us now carry out the simulation in simple one dimensional slab geometry, for which y and z are ignorable coordinates, $\hat{b}_0 = \theta\hat{x} + \hat{z}$, $x_\parallel = x/\theta$, $\theta \ll 1$ and $\kappa_\alpha = \kappa_n = \kappa_n \hat{y}$. Thus, from Eq. (14).

$$\frac{dx_\parallel}{dt} = v_\parallel \tag{70}$$

gives the equation for the velocity and, from Eq. (15),

$$\frac{dv_\parallel}{dt} = -s_\alpha v_{t\alpha}^2 \frac{\partial \psi}{\partial x_\parallel}, \qquad (71)$$

describes the acceleration. The particle weight equation is

$$\frac{dw_\alpha^{DNA}}{dt} = (1 - w_\alpha^{DNA}) \left[s_\alpha \frac{\partial \psi}{\partial t} - \left(\kappa_n - \frac{3}{2}\kappa_{T\alpha} + \frac{1}{2}\kappa_{T\alpha} \frac{v_\parallel^2 + v_\perp^2}{v_{T\alpha}} \right) \frac{\partial \psi}{\partial x} \right] \qquad (72)$$

Eqs. (45) and (46) are the field equations. The perturbed particle distribution is given by Eq. (39).

Figures 1-3 show the results for the simulations of shear-Alfvén waves, finite-β modified drift waves and finite-β modified ITG (η_I) modes, respectively. In these simulations $T_i/T_e = 1$, $k_\perp \rho_i = 0.4$ and $k_\parallel/k_\perp = 0.01$. For all values of β except $\beta = 0.1$, the time step $\Delta t \Omega_i = 0.2$, grid size $\Delta x/\rho_s = 0.0625$, and the number of particles for each species $n_p = 10946$ were chosen. For the case of $\beta = 0.1$ the time step was reduced to $\Delta t \Omega_i = 0.1$, and the number of particles for each species was increased to $n_p = 28657$. For the chosen simulation parameters the ratio of electron skin depth to the ion gyro-radius is $\delta_e/\rho_s = 0.07$.

Specifically, for damped shear-Alfvén oscillations, Fig. 1 shows the logarithmic plots of the normalized electric field potential ψ as function of time $\Omega_i t$ for $T_i/T_e = 1$, $\kappa_n = 0$ and $\kappa_{Ti} = \kappa_{Te} = 0.0$ for different values of plasma β. Numerical solution of exact dispersion relation Eq. (67) gives shear-Alfvén wave frequencies and damping rates: for $\beta = 0.1\%$: $(\omega + i\gamma)_{th}/\Omega_i = 0.13 - 0.0081i$ while the simulation result is $(\omega + i\gamma)_{sm}/\Omega_i = 0.13 - 0.0079i$; for $\beta = 1\%$: $(\omega + i\gamma)_{th}/\Omega_i = 0.042 - 0.00089i$ while the simulation result is $(\omega + i\gamma)_{sm}/\Omega_i = 0.042 - 0.00093i$; for $\beta = 3\%$: $(\omega + i\gamma)_{th}/\Omega_i = 0.024 - 0.00031i$ while the simulation result is $(\omega + i\gamma)_{sm}/\Omega_i = 0.025 - 0.00033i$; for $\beta = 10\%$: $(\omega + i\gamma)_{th}/\Omega_i = 0.013 - 0.00013i$ while the simulation result is $(\omega + i\gamma)_{sm}/\Omega_i = 0.013 - 0.00014i$.

For finite-β modified drift waves, Fig. 2 shows logarithmic plot of normalized electric field potential ψ as function of time $\Omega_i t$ for $T_i/T_e = 1$, $\kappa_n = 0.1$ and $\kappa_{Ti} = \kappa_{Te} = 0.0$ for different values of plasma β. Numerical solution of exact dispersion relation Eq. (67) gives finite-β modified drift waves frequencies and growth rates : for $\beta = 0.1\%$: $(\omega + i\gamma)_{th}/\Omega_i = 0.035 + 0.001i$ while the simulation result is $(\omega + i\gamma)_{sm}/\Omega_i = 0.033 + 0.001i$; for $\beta = 1\%$: $(\omega + i\gamma)_{th}/\Omega_i = 0.03 + 0.00087i$ while the simulation result is $(\omega + i\gamma)_{sm}/\Omega_i = 0.03 + 0.0009i$; for $\beta = 3\%$: $(\omega + i\gamma)_{th}/\Omega_i = 0.021 + 0.00022i$ while the simulation result is $(\omega + i\gamma)_{sm}/\Omega_i = 0.022 + 0.00024i$; for $\beta = 10\%$: $(\omega + i\gamma)_{th}/\Omega_i = 0.012 + 0.0i$ while the simulation result is $(\omega + i\gamma)_{sm}/\Omega_i = 0.0125 + 0i$.

For finite-β modified ITG modes, Fig. 3 shows logarithmic plot of normalized electric field potential ψ as function of time $\Omega_i t$ for $T_i/T_e = 1$, $\kappa_n = 0$ and $\kappa_{Ti} = \kappa_{Te} = 0.4$ for different values
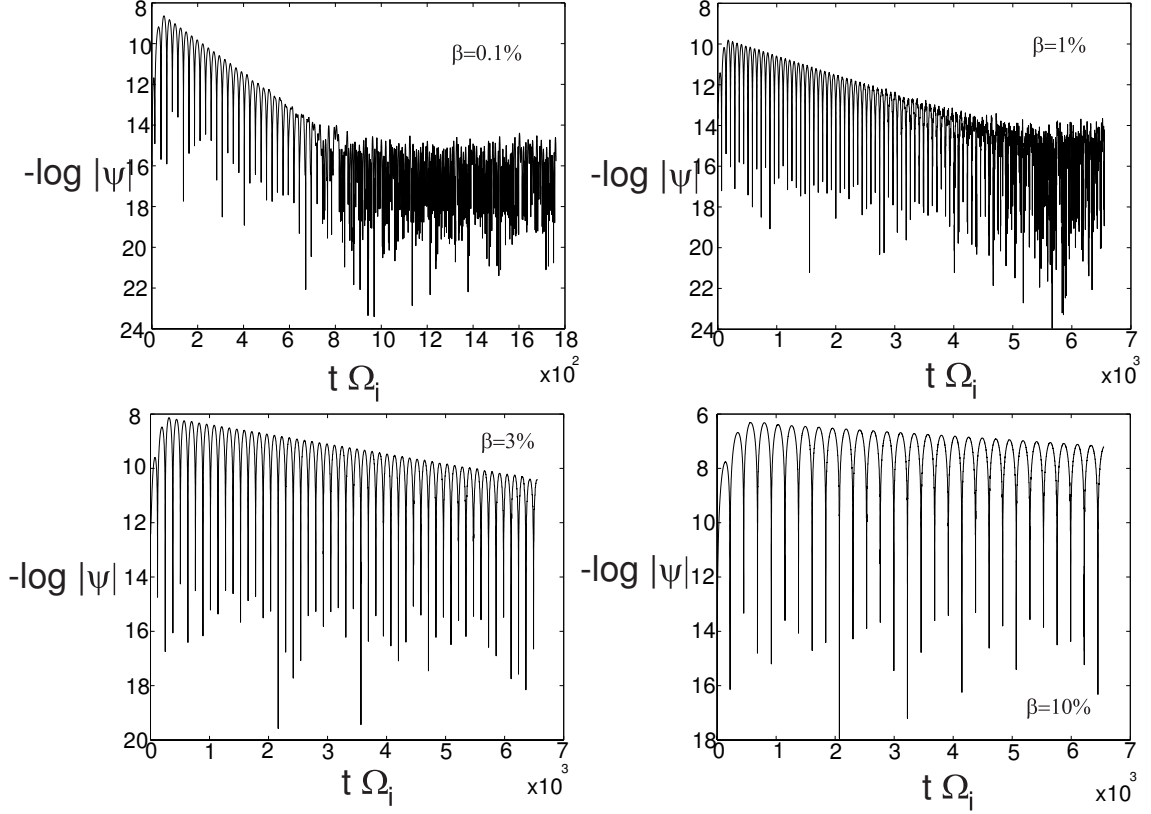
FIG. 1: Logarithmic plot of normalized electric field potential ψ for shear-Alfevn waves as function of time $\Omega_i t$ for $T_i/T_e = 1$, $\kappa_n = 0$, $\kappa_{Ti} = \kappa_{Te} = 0.0$ and plasma $\beta = 0.1, 1.0, 3.0$, and 10.0%.

of plasma β. Numerical solution of dispersion relation Eq. (67) gives finite-β modified η_I ITG modes wave frequencies and growth rates : for $\beta = 0.1\%$: $(\omega + i\gamma)_{th}/\Omega_i = -0.0057 + 0.0093i$ while the simulation result is $(\omega + i\gamma)_{sm}/\Omega_i = -0.0055 + 0.0082i$; for $\beta = 1\%$: $(\omega + i\gamma)_{th}/\Omega_i = -0.0057 + 0.0093i$ while the simulation result is $(\omega + i\gamma)_{sm}/\Omega_i = -0.0055 + 0.0082i$; for $\beta = 5\%$: $(\omega + i\gamma)_{th}/\Omega_i = -0.0059 + 0.0094i$ while the simulation result is $(\omega + i\gamma)_{sm}/\Omega_i = -0.0058 + 0.0086i$ and for $\beta = 10\%$: $(\omega + i\gamma)_{th}/\Omega_i = -0.0059 + 0.0096i$ while the simulation result is $(\omega + i\gamma)_{sm}/\Omega_i = -0.0058 + 0.0095i$. It is well known that ITG modes are stabilized by finite β effects only if finite gyro-radius effects are included. The equations that include finite gyro-radius effects are derived in Appendix C. The results of simulations using these equations agree well with the solution of eighenmode equation. As an illustration, Figure 4 shows the plot of normalized electric field potential ψ as function of time $\Omega_i t$ for $T_i/T_e = 1$, $\kappa_n = 0.1$ and $\kappa_{Ti} = \kappa_{Te} = $
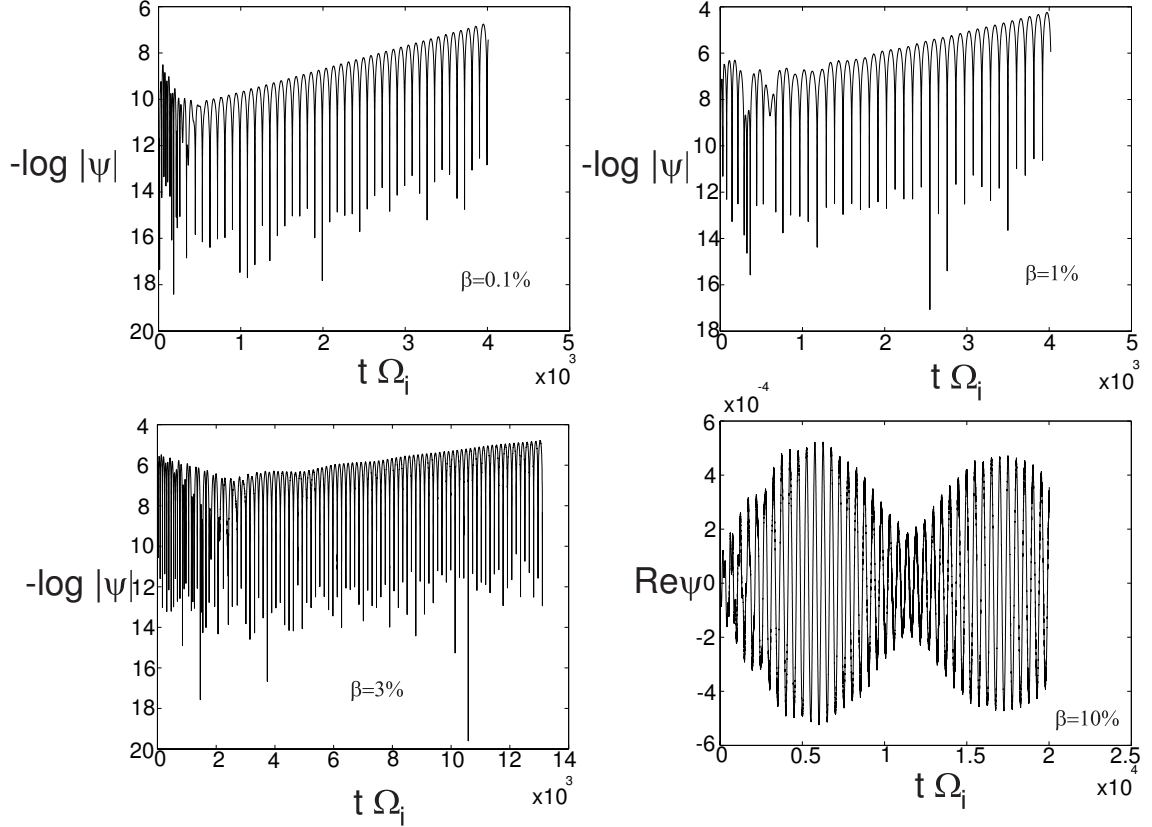
FIG. 2: Logarithmic plot of normalized electric field potential ψ for drift instabilities as function of time $\Omega_i t$ for $T_i/T_e = 1$, $\kappa_n = 0.1$, $\kappa_{Ti} = \kappa_{Te} = 0.0$ and plasma $\beta = 0.1, 1.0, 3.0,$ and 10.0%.

0.4 for $\beta = 10\%$. The numerical growth rate and the oscillation frequency of the mode agree well with numerical solution of exact dispersion relation with finite gyro-radius effects included: $(\omega + i\gamma)_{th}/\Omega_i = -0.003 + 0.0023i$ while the simulation result is $(\omega + i\gamma)_{sm}/\Omega_i = -0.003 + 0.002i$.

To illustrate the influence of the spatial resolution on the accuracy of the simulations and the resolution of the cancellation problem discussed above, we plot in Figure 5 the results of simulations of ITG mode with $\kappa_n = 0$, $\kappa_{Ti} = \kappa_{Te} = 0.4$, $n_p = 46368$, $\Delta t \Omega_i = 0.1$, $k_\perp \rho_i = 0.4$, $k_\parallel/k_\perp = 0.01$, $T_e/T_i = 1$. In Fig. 5 the red (I) curve corresponds to simulation where the skin-depth was resolved with $\Delta x/\rho_s = 0.0625$ and $A = 1$ was used in field equation (57) for $\partial\psi/\partial t$. The green line (II) corresponds to the same simulation but with skin-depth not resolved $\Delta x/\rho_s = 1.0$. Note the wrong frequency and wrong growth rate of ITG mode due to incomplete cancellation of large terms in Eq. (57). The black (III) and blue (IV) lines are result of simulation where the skin-depth was not resolved, $\Delta x/\rho_s = 1.0$, but the equation for $\partial\psi/\partial t$, Eq. (57), was corrected to insure the cancellation of large terms as explained in Sec. V and Appendix A. The
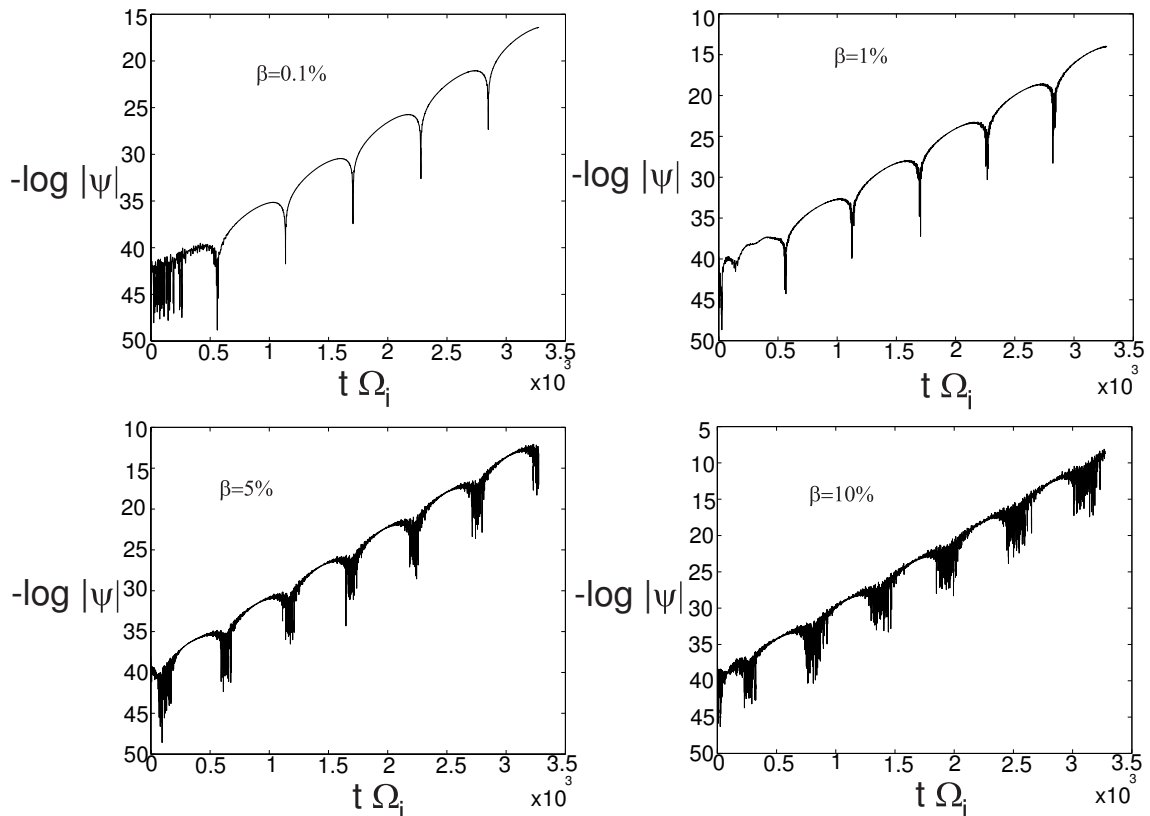
FIG. 3: Logarithmic plot of normalized electric field potential ψ as function of time $\Omega_i t$ for $T_i/T_e = 1$, $\kappa_n = 0$, $\kappa_{Ti} = \kappa_{Te} = 0.4$ and and plasma $\beta = 0.1, 1.0, 5.0$, and 10.0%.

differences between black (III) and blue (IV) lines are due to the use of inconsistent definition $\nabla_x \psi = i k_x \psi$ (black line III) instead of correct one $[\psi(x + dx) - \psi(x - dx)]/2/dx$ (blue line IV) in the field equation for $\partial\psi/\partial t$. That was needed to be consistent with the same term in equation for weights (last term in Eq. (37)). By correcting those large terms in Eq. (57) for $\partial\psi/\partial t$, the simulation results are in good agreement with theory without the need to resolve the skin-depth.

VI. CONCLUSIONS

In this paper, we have extended the previously developed split-weight simulation scheme [4] to the finite-β gyro-kinetic plasmas with background inhomogeneity. In the new double-split-weight scheme, the additional adiabatic response to the quasi-static bending of the magnetic field lines due to magnetic field perturbation is analytically separated out, so that full inhomogeneity gradient, background plus perturbation, is transverse to the direction of total magnetic field, background
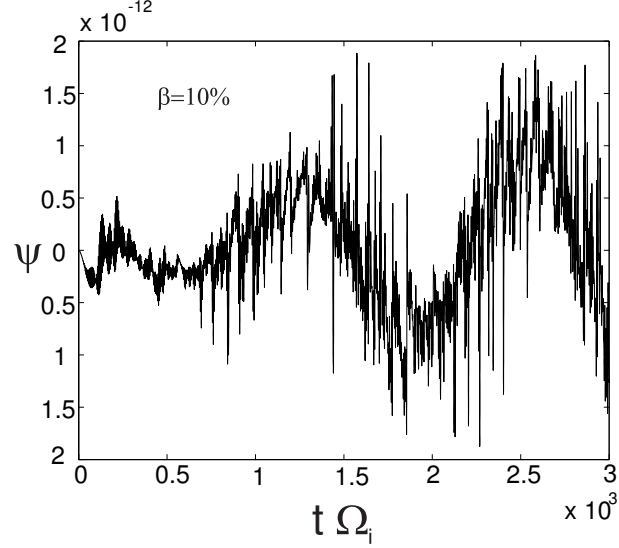
FIG. 4: Plot of normalized electric field potential ψ as function of time $\Omega_i t$ for $T_i/T_e = 1$, $\kappa_n = 0.1$, $\kappa_{Ti} = \kappa_{Te} = 0.4$ and plasma $\beta = 10.0\%$ obtained taking into account the finite Larmor radius effects as described in Appendix C.
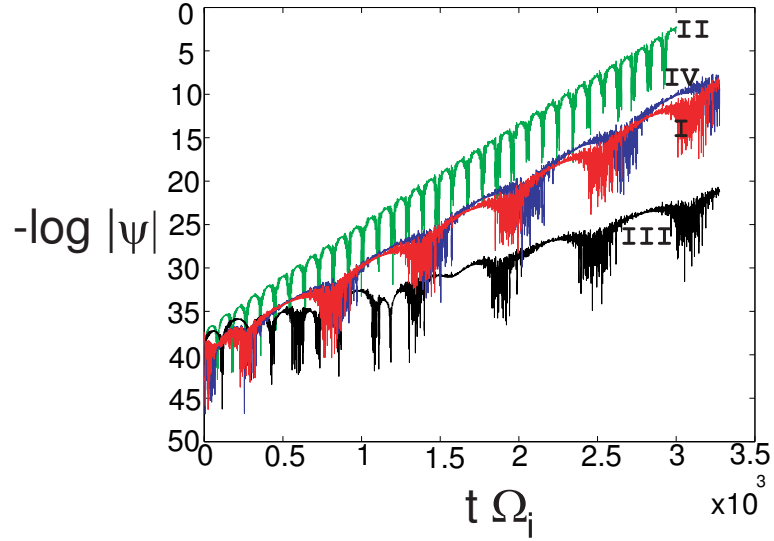
FIG. 5: Logarithmic plot of normalized electric field potential ψ as function of time $\Omega_i t$ for $T_i/T_e = 1$, $\kappa_n = 0$, $\kappa_{Ti} = \kappa_{Te} = 0.4$ and and plasma $\beta = 10.0\%$. Here, $\Delta x/\rho_s = 0.0625$ and $A = 1$ is used for red (I) line; $\Delta x/\rho_s = 1.$ and $A = 1$ is used for green (II) line, and $\Delta x/\rho_s = 1.0$ and A given by Eq. (A6) is used for black (III) and blue (IV) lines. The definition $\nabla_x \psi = ik_x \psi$ (black (III) line) and $\nabla_x \psi = [\psi(x + dx) - \psi(x - dx)]/2/dx$ (blue (IV) line) are used in the field equation (57) for $\partial \psi/\partial t$.

plus perturbation, as in Eq. (36). Formally, such separation removed large terms proportional to electron velocity from electron Vlasov equation, which allowed for a larger time-step in simulations of low-frequency phenomena in finite-β gyrokinetic plasmas. The resulting equations have been implemented in 2D shearless slab-geometry particle-in-cell gyrokinetic code which was used to study shear-Alfvén waves and finite-β modified drift waves and ion temperature gradient (ITG) modes and instabilities in the long-wavelength limit $k_\perp^2 \rho_i^2 \ll 1$. The finite Larmor radius effects for $k_\perp^2 \rho_i^2 \sim 1$ can be easily recovered as shown in Appendix C and demonstrated by simulating the finite-beta stabilization of ITG modes for $\beta = 10\%$ [see Fig. 4].

In this paper, we have paid special attention to high-β regime $\beta \gg m_e/m_i$ which is known to be especially difficult to simulate using gyrokinetic codes. For particle-in-cell codes this is known as "cancellation problem", and has been a subject of numerous studies [3, 10]. In early efforts to simulate shear-Alfvén waves [3] it was observed that an electron skin-depth $\delta_e \ll \rho_i$ had to be resolved in the plane transverse to magnetic field in order to eliminate numerical instability. On the other hand, it was shown that the accurate numerical cancellation of large terms in Ampere's law also eliminates the numerical instability [10]. We have shown in this paper that both views are consistent with each other, and indeed the inaccuracy in numerical evaluation of Ampere's law is proportional to $(\Delta x/\delta_e)^2$ and therefore is made small by resolving the electron skin-depth $\Delta x < \delta_e$. It is often prohibitively expensive to resolve the electron skin-depth everywhere in simulations domain, unless it becomes necessary. e.g., near rational surfaces. Using the analysis of numerical cancellation problem given in Sec. V and Appendix A, we have shown how to correctly modify the equation representing the Ampere's law in our method which leads to the accurate cancellation of large terms and eliminates the need for such fine scale resolution. The extension of the present formalism to include sheared geometry for studying tearing modes will be presented in a subsequent study. Here we just note that our scheme is non-perturbative, as such, it allows simulations of the modes with arbitrary values of $\omega/(k_\parallel v_{te})$. Such feature is absolutely necessary for accurate numerical representation of tearing modes near rational surfaces in tokamaks where $\omega/(k_\parallel v_{te}) \to \infty$ [See Appendix B where our scheme is compared with the perturbative "hybrid method" of Ref. [12]].

Recently, shearless ITG modes based on an extended MHD model [26] have been investigated for the purpose of incorporating kinetic effects in hybrid MHD codes. Our study here represent an approach from the opposite direction. Namely, the study of drift waves and ITG modes kinetically in our paper is for the purpose of extending gyro-kinetics codes into the MHD regime.

Acknowledgement

Appendix A: Resolution of the Cancellation Problem

Let us describe the derivation of Eq. (57) as follows. To obtain Eq. (46) we first differentiate Eq. (45) with respect to time and then use the time derivatives of $d\delta g_\alpha/dt$ from Eq. (37). The form of Eq. (37) assumes that particles are localized, i.e, contributions to the charge density at $\mathbf{x}$ from the particle at the location $\mathbf{x}_\alpha$ is related to the delta-function, $\delta(\mathbf{x} - \mathbf{x}_\alpha)$. In the PIC simulations [28], the field quantities such as ψ are defined on the grid as $\psi(\mathbf{X}_p) \equiv \psi_p$ at a location $\mathbf{X}_p \equiv (X_{p1}, X_{p2}, X_{p3}) = (p_1\Delta x_1, p_2\Delta x_2, p_3\Delta x_3)$, where $\Delta\mathbf{x} \equiv (\Delta x_1, \Delta x_2, \Delta x_3)$ is the grid and $\mathbf{p} \equiv (p_1, p_2, p_3)$ is a vector with integer components $p_i = 0, 1, 2, \ldots, (N_i - 1)$ with $i = 1, 2, 3$, $N_i = L_i/\Delta x_i$ and L_i is the system length along i-direction. The field at the particle location $\mathbf{x}_{\alpha j}$ is interpolated from the grid using a weighting function $S(\mathbf{x})$ by $\psi(\mathbf{x}_{\alpha j}) = \Delta V \sum_p \psi_p S(\mathbf{X}_p - \mathbf{x}_{\alpha j})$, where ΔV is the volume of the grid cell. In turn, the contribution to the particle density at the grid location $\mathbf{X}_p$ coming from the particle located at position $\mathbf{x}_{\alpha j}$ is given by the same weighting function and is proportional to $w_{\alpha j}S(\mathbf{X}_p - \mathbf{x}_{\alpha j})$ with the total density from all particles given by $\delta n_\alpha(\mathbf{X}_p) = \int dv_\| d\mu \delta g_\alpha(\mathbf{X}_p, v_\|, \mu) = \sum_{\alpha j} w_{\alpha j}S(\mathbf{X}_p - \mathbf{x}_{\alpha j})$.

As the result of such nonlocal weighting, the grid version of Eq. (46) can be written as

$$\left[(\nabla_\perp^2 - 1 - \tau)\frac{\partial\psi}{\partial t}\right]_p = -\beta(\hat{\mathbf{b}}_0 \cdot \nabla)\int v_\|^3(\delta g_i - \delta g_e)d\mu dv_\| + (\hat{\mathbf{b}}_0 \cdot \nabla)\int v_\|(\delta g_i - \delta g_e)d\mu dv_\|$$

$$+(n_0\Delta V)\sum_l \int d\mathbf{x} S(\mathbf{X}_p - \mathbf{x})S(\mathbf{X}_l - \mathbf{x})\left\{(\beta\frac{m_i}{m_e} + \beta - 1 - \tau)\frac{\partial\psi_l}{\partial t} + \right.$$

$$\left. \beta(\nabla\psi)_l \times \hat{\mathbf{b}}_0 \cdot \left[\frac{m_i}{m_e}(\boldsymbol{\kappa}_n + \boldsymbol{\kappa}_{Te}) - \frac{1}{\tau}(\boldsymbol{\kappa}_n + \boldsymbol{\kappa}_{Ti})\right]\right\}, \tag{A1}$$

where we have replaced the summation over particles with integration over space $\sum_j \to n_0 \int d\mathbf{x}$ and l is the grid location index. Note that Eq. (A1) is reduced to Eq. (46) for the weighting factor

$S(x) = \delta(x)$ if we use the identity $\sum_l \delta(\mathbf{X}_p - \mathbf{X}_l)\Delta V = \sum_l \delta_{pl} = 1$, where δ_{pl} is the Kronecker symbol, and recall that in our normalized units $n_0 \equiv 1$.

Equation (A1) is simplified by the use of Fourier series where grid quantities such as ψ_p are expressed as

$$\psi_p = \frac{1}{V} \sum_s \bar{\psi}_s e^{i\mathbf{k}_s \mathbf{X}_p}, \tag{A2}$$

where $\mathbf{k}_s = \mathbf{s}k_L$, $\mathbf{s}$ is the vector with integer components $s_i = 0, \pm 1, \pm 2, \ldots, \pm(N_i - 1)$ with $i = 1, 2, 3$, $N_i = L_i/\Delta x_i$, and $\mathbf{k}_L = 2\pi(1/L_1, 1/L_2, 1/L_3)$. Using the relationship of

$$\int d\mathbf{x} S(\mathbf{X}_p - \mathbf{x}) S(\mathbf{X}_l - \mathbf{x}) = \frac{1}{V} \sum_\mathbf{s} \left[\sum_\mathbf{p} |\bar{S}(\mathbf{k}_s - \mathbf{p}k_g)|^2 \right] e^{i\mathbf{k}_s(\mathbf{X}_p - \mathbf{X}_l)}, \tag{A3}$$

where $\mathbf{k}_g = 2\pi(1/\Delta x_1, 1/\Delta x_2, 1/\Delta x_3)$ and $\mathbf{p}$ is the vector with integer components $p_i = 0, \pm 1, \pm 2, \ldots$ with $i = 1, 2, 3$, and Fourier transform of weighting function

$$\bar{S}(\mathbf{k}) \equiv \int d\mathbf{x} S(\mathbf{x}) e^{-i\mathbf{k}\mathbf{x}}, \tag{A4}$$

Equation (A1) in Fourier space can be written as

$$\left[\nabla_\perp^2(\mathbf{k}_s) - 1 - \tau \right] \frac{\partial \bar{\psi}_s}{\partial t} = \tag{A5}$$
$$-\beta(\hat{\mathbf{b}}_0 \cdot \nabla(\mathbf{k_s}) \int v_\parallel^3 (\delta g_i - \delta g_e) d\mu dv_\parallel + (\hat{\mathbf{b}}_0 \cdot \nabla(\mathbf{k_s}) \int v_\parallel (\delta g_i - \delta g_e) d\mu dv_\parallel$$
$$+A(\mathbf{k}_s) \left\{ (\beta \frac{m_i}{m_e} + \beta - 1 - \tau) \frac{\partial \bar{\psi}_s}{\partial t} + \beta \nabla(\mathbf{k}_s) \times \hat{\mathbf{b}}_0 \cdot \left[\frac{m_i}{m_e}(\boldsymbol{\kappa}_n + \boldsymbol{\kappa}_{Te}) - \frac{1}{\tau}(\boldsymbol{\kappa}_n + \boldsymbol{\kappa}_{Ti}) \right] \bar{\psi}_s \right\},$$

where $A(\mathbf{k}) \equiv \sum_\mathbf{p} |\bar{S}(\mathbf{k} - \mathbf{p}k_g)|^2$. Note that Eq. (A5) differs from Eq. (46) in Fourier space by a form factor $A(\mathbf{k}) \neq 1$ due to finite size grid. For a weighting function which corresponds to a linear interpolation of the field from closest grid neighbour nodes, the form-factor $A(\mathbf{k})$ can be approximated by the first term in the sum, and is given by

$$A(\mathbf{k}) \approx \left[dif\left(\frac{k_1 \Delta x_1}{2}\right) dif\left(\frac{k_2 \Delta x_2}{2}\right) dif\left(\frac{k_3 \Delta x_3}{2}\right) \right]^4, \tag{A6}$$

where $dif(\theta) \equiv \sin\theta/\theta$ is a *diffraction function*.

For $\mathbf{k}^2 \Delta \mathbf{x}^2 \ll 1$, $A(\mathbf{k}) \approx 1 - [(k_1 \Delta x_1)^2 + (k_2 \Delta x_2)^2 + (k_3 \Delta x_3)^2]/6$ and we can use the value $A = 1$ in Eq. (A5) everywhere except where it is multiplied by large factor $\beta(m_i/m_e)$, i.e.,

$$\left[\nabla_\perp^2(\mathbf{k}_s) - \beta - \beta \frac{m_i}{m_e} A(\mathbf{k}_s) \right] \frac{\partial \bar{\psi}_s}{\partial t} = -\beta \hat{\mathbf{b}}_0 \cdot \nabla(\mathbf{k}_s) \int v_\parallel^3 (\delta g_i - \delta g_e) d\mu dv_\parallel \tag{A7}$$
$$+\hat{\mathbf{b}}_0 \cdot \nabla(\mathbf{k}_s) \int v_\parallel (\delta g_i - \delta g_e) d\mu dv_\parallel + \beta \nabla(\mathbf{k}_s) \times \hat{\mathbf{b}}_0 \cdot \left[A(\mathbf{k}_s) \frac{m_i}{m_e}(\boldsymbol{\kappa}_n + \boldsymbol{\kappa}_{Te}) - \frac{1}{\tau}(\boldsymbol{\kappa}_n + \boldsymbol{\kappa}_{Ti}) \right] \bar{\psi}_s.$$

For low-frequency modes such as ITG mode, the electrons response is adiabatic, and the electron velocity integrals will cancel the large terms proportional to $\beta m_i/m_e$ in Eq. (A7). The remaining terms will determine the mode frequency. If the approximation $A = 1$ is used in Eq. (A7), the cancellation will be incomplete, with the remaining terms proportional to $\beta(m_i/m_e)k_\perp^2\Delta x_\perp^2$ due to incomplete cancellation of adiabatic electron response in Eq. (A7). For the simulation to reproduce frequency correctly, the error introduced by this term must be smaller than the remaining terms such as the first term in Eq. (A7), $\nabla_\perp^2(\mathbf{k}_s) = -k_\perp^2$. This introduces the requirement that the grid size be smaller then the skin-depth $\Delta x_\perp \ll [\beta(m_i/m_e)]^{-1/2} \equiv \delta_e$. The numerical instability can then be completely removed if the correct form for the formfactor $A(\mathbf{k})$ given by Eq. (A6) is used in Eq. (A7).

The scheme presented here is similar to that of Chen and Parker [10], but is different in implementation.

Appendix B: Relationship to the Hybrid Method

In present work, the gyrokinetic Vlasov equation, Eq. (37), and the associated field equations, Eqs. (45) and (46), have been used as a complete set of equations describing the self-consistent evolution of fields and particles. In this appendix we will illustrate the relationship of our approach, based on the original split-weight scheme [4], with the hybrid scheme developed by Lin and Chen [12]. In the approach presented here the fields ψ and $\partial\psi/\partial t$ are the independent fields satisfying system of Eqs. (45) and (46). Equation (46) was derived by taking the time derivative of Eq. (45) and using the gyrokinetic Vlasov equation of

$$\frac{\partial}{\partial t}g_\alpha = -v_\parallel\frac{\partial}{\partial x_\parallel}g_\alpha - \left[s_\alpha\frac{\partial\psi}{\partial t} - \nabla\psi \times \hat{\mathbf{b}}_0 \cdot \boldsymbol{\kappa}_\alpha\right]F_{0\alpha} \tag{B1}$$

to eliminate $\partial g_\alpha/\partial t$. Note that in the last step we replaced the small term $\partial g_\alpha/\partial t$ in terms of combination of large terms (for low-frequency waves $\partial/\partial t \sim \omega \ll k_\parallel v_\parallel$). This way the cancellation problem was introduced into the field equations, which was solved by us using the method described in Appendix A. The advantage of this approach is that static system of equations needs to be solved on every time-step and, therefore, the field solvers that have been developed for electrostatic problems with zero β can be easily adopted to electromagnetic problems with non-zero β.

A different approach was taken by Lin and Chen [12]. For simplicity, we will only illustrate

this approach using the example with zero background gradients and assuming immobile ions. These restrictions can be easily removed by including the rest of the terms, if desired. By taking a second spatial derivative of Eq. (45) along the magnetic field we obtain

$$(\nabla_\perp^2 - 1)\frac{\partial^2}{\partial x_\parallel^2}\psi = -\beta \int \left(v_\parallel \frac{\partial}{\partial x_\parallel}\right)^2 g_e d\mu dv_\parallel + \frac{\partial^2}{\partial x_\parallel^2}\int g_e d\mu dv_\parallel. \tag{B2}$$

Next, we use the gyrokinetic Vlasov equation for g_e,

$$v_\parallel \frac{\partial}{\partial x_\parallel} g_e = -\frac{\partial}{\partial t} g_e - \frac{\partial}{\partial t}\psi F_{0e}, \tag{B3}$$

twice to eliminate $(v_\parallel \partial/\partial x_\parallel)^2 g_e$ in Eq. (B2) and obtain the wave-like equation of the form,

$$\beta \frac{\partial^2}{\partial t^2}\left[\psi + \int g_e d\mu dv_\parallel\right] = \frac{\partial^2}{\partial x_\parallel^2}\left[\psi + \int g_e d\mu dv_\parallel\right] - \nabla_\perp^2 \frac{\partial^2}{\partial x_\parallel^2}\psi. \tag{B4}$$

Introducing the full perturbed electron density

$$n_e = \psi + \int g_e d\mu dv_\parallel, \tag{B5}$$

we can rewrite Eqs. (B4) and (B3) for n_e and g_e as coupled set of equations

$$\beta \frac{\partial^2}{\partial t^2}n_e = (1 - \nabla_\perp^2)\frac{\partial^2}{\partial x_\parallel^2}n_e + \nabla_\perp^2 \frac{\partial^2}{\partial x_\parallel^2}\int g_e d\mu dv_\parallel. \tag{B6}$$

$$\frac{d}{dt}g_e = -\left(\frac{\partial}{\partial t}n_e\right) F_{0e} + \boxed{\left(\tfrac{\partial}{\partial t}\int g_e d\mu dv_\parallel\right) F_{0e}}. \tag{B7}$$

It follows from Eq. (B6) that the wave frequency is given by $\omega^2 \approx v_A^2 k_\parallel^2(1 + k_\perp^2)$ with $v_A^2 = 1/\beta$ assuming that non-adiabatic correction are small

$$\frac{\int g_e d\mu dv_\parallel}{n_e} \approx \frac{\omega}{k_\parallel v_{te}} \approx \frac{v_A}{v_{te}} \approx \frac{1}{(\beta m_i/m_e)^{1/2}} \ll 1. \tag{B8}$$

In that case one can also neglect the last term (boxed) in Eq. (B7) compared to the second term as was also done in Ref. [12]. Equations (B6) and (B7) constitute a complete set of equations describing the alfven dynamics with kinetic electron contribution represented by the terms proportional to g_e. Equations (B6) and (B7) without the boxed term are equivalent to equations used in Ref. [12]

Note that this method only works for large β so that $(\beta m_i/m_e)^{1/2} \gg 1$. There are no problems with cancellation of large terms proportional to $(\beta m_i/m_e)^{1/2} \gg 1$ in this approach. The numerical constraints in solving Eqs. (B6) and (B7) are

$$\omega \Delta t \sim k_\parallel v_A \Delta t \ll 1, \quad k_\parallel v_{te} \Delta t \sim \left(\frac{v_{te}}{v_A}\right) k_\parallel v_A \Delta t \sim \left(\beta \frac{m_i}{m_e}\right)^{1/2} \omega \Delta t < 1, \tag{B9}$$

where the first constraint is needed to accurately resolve the mode frequency and the second is to accurately reproduce the Landau damping of the wave.

As it is clear from this presentation, Ref. [12] approach is designed for low-frequency alfvenic dynamics only, $\omega/k_\parallel \ll v_{te}$, and, therefore, does not work near the rational surfaces for studying tearing modes. Furthermore, even though the final equations do not contain large parameters proportional to $(\beta m_i/m_e)^{1/2} \gg 1$, Eq. (B6) has the form of a wave equation and it may be difficult to implement in the codes designed with static field solvers.

Appendix C: Finite Larmor Radius Effects on ITG Modes

To take into account the finite Larmor radius effects for $k_\perp \rho_i \sim 1$, we need to re-write the governing equations, Eqs. (40) and (41) in k-space as [2]

$$\hat{Q}\phi - (1 + \tau\hat{\Gamma}_0)\psi = -S_0 - \int dx_\parallel \left[(\hat{\Gamma}_0 - 1)\boldsymbol{\kappa}_n + \boldsymbol{\kappa}_{Ti}(\hat{\Gamma}^* - \hat{\Gamma}_0)\right] \cdot (\nabla A_\parallel \times \mathbf{b}_0), \qquad \text{(C1)}$$

$$\nabla_\perp^2 A_\parallel = -\beta S_1, \qquad \text{(C2)}$$

where

$$S_n \equiv \int v_\parallel^n (\hat{J}_0 \delta g_i - \delta g_e) dv_\parallel d\mu, \qquad \text{(C3)}$$

and, from Eq. (37), the equations for the non-adiabatic part of the distribution function for the electrons and ions are

$$\frac{d\delta g_e}{dt} = -\frac{\partial\psi}{\partial t} - (\nabla\psi \times \mathbf{b}_0) \cdot \boldsymbol{\kappa}_e$$
$$\frac{d\delta g_i}{dt} = \tau\frac{\partial\bar{\psi}}{\partial t} - (\nabla\bar{\psi} \times \mathbf{b}_0) \cdot \boldsymbol{\kappa}_i, \qquad \text{(C4)}$$

where $\bar{\psi} = \hat{J}_0\psi$, $\boldsymbol{\kappa}_\alpha \equiv -(\partial F_{0\alpha}/\partial\mathbf{x})/F_{0\alpha} = \boldsymbol{\kappa}_n - \frac{3}{2}\boldsymbol{\kappa}_{T\alpha} + \frac{1}{2}\boldsymbol{\kappa}_{T\alpha}(v_\parallel^2 + v_\perp^2)/v_{t\alpha}^2$, $\boldsymbol{\kappa}_n \equiv -dlnn_0/d\mathbf{x}$, and $\boldsymbol{\kappa}_{T\alpha} \equiv -dlnT_{0\alpha}/d\mathbf{x}$ represent the zeroth-order inhomogeneities and $F_{0\alpha} \equiv (1/\sqrt{2\pi}v_{t\alpha}^3)exp[-(v_\parallel^2 + v_\perp^2)/2v_{t\alpha}^2]$ is the background Maxwellian. Definitions of operators in Eq. (C1)-(C4) are

$$b \equiv \left(\frac{k_\perp^2}{\tau}\right) = -\frac{\nabla_\perp^2}{\tau}, \quad c \equiv k_\perp(2\mu)^{1/2},$$
$$\hat{\Gamma}_0 = I_0(b)e^{-b},$$
$$\hat{\Gamma}_1 = I_1(b)e^{-b},$$

$$\hat{Q} \equiv -\tau[1 - \hat{\Gamma}_0],$$

$$\hat{\Gamma}^* \equiv \hat{\Gamma}_0 - b[\hat{\Gamma}_0 - \hat{\Gamma}_1],$$

$$\hat{J}_0 = J_0(c), \tag{C5}$$

where J_0 is zeroth-order Bessel function, I_0 and I_1 are modified Bessel functions of zeroth and first order respectively. Using Eqs. (C4) we obtain the relations between S_n's:

$$\frac{\partial S_1}{\partial t} = -\frac{\partial S_2}{\partial x_\parallel},$$

$$\frac{\partial S_2}{\partial t} = -\frac{\partial S_3}{\partial x_\parallel} + \left(\hat{\Gamma}_0 + \frac{m_i}{m_e}\right)\frac{\partial \phi}{\partial t}$$

$$+ \left[\frac{m_i}{m_e}(\boldsymbol{\kappa}_n + \boldsymbol{\kappa}_{Te}) - \frac{1}{\tau}(\boldsymbol{\kappa}_n \hat{\Gamma}_0 + \boldsymbol{\kappa}_{Ti}\hat{\Gamma}^*)\right] \cdot (\nabla \psi \times \mathbf{b}_0). \tag{C6}$$

Substituting Eqs. (C6) and

$$\phi = \psi - \frac{\partial_t}{\partial_\parallel}A = \psi - \frac{\partial_t}{\partial_\parallel \nabla_\perp^2}\nabla_\perp^2 A$$

$$= \psi + \beta\left[\frac{\partial_t S_1}{\partial_\parallel \nabla_\perp^2}\right] = \psi - \frac{\beta}{\nabla_\perp^2}S_2 \tag{C7}$$

into Eqs. (C2) we obtain the finial set of two field equations for ψ and $\partial_t \psi$ as

$$(1 + \tau)\partial_\parallel \psi = \partial_\parallel(S_0 - \beta\frac{\hat{Q}}{\nabla_\perp^2}S_2) + \left[(\hat{\Gamma}_0 - 1)\boldsymbol{\kappa}_n + \boldsymbol{\kappa}_{Ti}(\hat{\Gamma}^* - \hat{\Gamma}_0)\right] \cdot (\nabla A \times \mathbf{b}_0) \tag{C8}$$

and

$$\left[\hat{Q} - (\hat{\Gamma}_0 + \frac{m_i}{m_e})\beta\frac{\hat{Q}}{\nabla_\perp^2}\right]\partial_t \psi = \partial_\parallel(S_1 - \beta\frac{\hat{Q}}{\nabla_\perp^2}S_3) \tag{C9}$$

$$- \frac{\beta}{\nabla_\perp^2}\left[(\hat{\Gamma}_0 - 1)\boldsymbol{\kappa}_n + \boldsymbol{\kappa}_{Ti}(\hat{\Gamma}^* - \hat{\Gamma}_0)\right] \cdot (\nabla S_2 \times \mathbf{b}_0)$$

$$+ \left[(\hat{\Gamma}_0 - 1)\boldsymbol{\kappa}_n + \boldsymbol{\kappa}_{Ti}(\hat{\Gamma}^* - \hat{\Gamma}_0) + \beta\frac{\hat{Q}}{\nabla_\perp^2}\left\{\frac{m_i}{m_e}(\boldsymbol{\kappa}_n + \boldsymbol{\kappa}_{Te}) - \frac{1}{\tau}(\boldsymbol{\kappa}_n\hat{\Gamma}_0 + \boldsymbol{\kappa}_{Ti}\hat{\Gamma}^*)\right\}\right] \cdot (\nabla \psi \times \mathbf{b}_0).$$

Here, $\partial_t \equiv \partial/\partial t$, $\partial_\parallel \equiv \partial/\partial x_\parallel = ik_\parallel$, $\nabla = i\mathbf{k}$, and $\nabla_\perp^2 = -k_\perp^2$. This set of equations has been used to obtain the results shown in Fig. 4 for $\beta = 10\%$, which, in comparison with the corresponding plot in Fig. 3, shows the importance of finite Larmor radius (FLR) effects on the stabilization of ITG modes.

---

[1] T. S. Hahm, W. W. Lee, A. Brizard, Phys. Fluids **31**, 1940 (1988).

[2] J. V. W. Reynders, Ph.D. thesis, Princeton University (1992).

[3] J. C. Cummings, Ph.D. thesis, Princeton University (1995).

[4] W. W. Lee, J. L. V. Lewandowski, T. S. Hahm and Z. Lin, Phys. Plasmas **8**, 4435 (2001).

[5] I. Manuilskiy and W. W. Lee, Phys. Plasmas, **7**, 1381 (2000).

[6] S. E. Parker, and W. W. Lee, Phys. Fluids B **5**, 77 (1993).

[7] H. Roos, M. Stynes and L. Tobiska, "Robust Numerical Methods for Singularly Perturbed Differential Equations," Springer, Germany (2008).

[8] G. I. Shishkin and L. P. Shishkina, "Difference Mathods for Singular Problems," Chapman & Hall/CRC Press (2009).

[9] F. Jenko, Comp. Phys. Comm. **125**, 196 (2000).

[10] Y. Chen and S. E. Parker, J. Comp. Phys. **189**, 463 (2003).

[11] J. Candy and R. E. Waltz, J. Comp. Phys. **186**, 545 (2003).

[12] Z. Lin and L. Chen, Phys. Plasmas **8**, 1447 (2001).

[13] Z. Lin, T. S. Hahm, W. W. Lee, W. M. Tang and R. White, *Science*, **281**, 1835 (1998).

[14] W. X. Wang, Z. Lin, W. M. Tang, W. W. Lee, S. Ethier, J. L. V. Lewandowski, G. Rewoldt, T. S. Hahm and J. Manickam, Phys. Plasmas **13**, 092505 (2006).

[15] W. W. Lee and H. Qin, Phys. Plasmas **10**, 3196 (2003).

[16] Y. Chen and S. E. Parker, J. Comp. Phys. **220**, 839 (2007).

[17] Y. Nishimura, Z. Lin and L. Chen, Comm. in Comp. Phys. **5**, 183 (2009).

[18] W. W. Lee, Phys. Fluids **26**, 556 (1983).

[19] W. W. Lee, J. Comp. Phys. **72**, 243 (1987).

[20] H. Strauss, Phys. Fluids **19**, 134 (1976).

[21] W. W. Lee, E. A. Startsev, and W. X. Wang, "A new split-weight scheme for finite-β gyrokinetic plasmas," Bull. Am. Phys. Soc. **52**, 338 (2007).

[22] Y. Nishimura, Z. LIn, W. X. Wang, Phys. Plasmas **14**, 042503 (2007).

[23] A. B. Langdon, J. Comput. Phys. **30**, 202 (1970).

[24] A. B. Langdon, J. Comput. Phys. **6**, 247 (1979).

[25] W. W. Lee and W. M. Tang, Phys. Fluids **31**, 612 (1988).

[26] D. D. Schnack, J. Cheng, D. C. Barnes and S. E. Parker, "Comparison of Kinetic and Extended MHD Computational Models for the Ion Temperature Gradient Instability in Slab Geometry," Phys. Plasmas (to appear).

[27] T. J. Jenkins, Ph.D. Thesis, Princeton University (2007).

[28] C. K. Birdsall, A. B. Langdon, "Plasma Physics via Computer Simulation", Taylor & Francis (2004).